Geological Society Of America Bulletin
May 2018, Volume 130 Issue 5-6 Pages 941-951
https://doi.org/10.1130/B31648.1
https://archimer.ifremer.fr/doc/00638/74990/

Phytoplankton contributions to the trace-element composition of Precambrian banded iron formations

Konhauser Kurt O. [1, *], Robbins Leslie J. [1], Alessi Daniel S. [1], Flynn Shannon L. [1], Gingras Murray K [1], Martinez Raul E. [2], Kappler Andreas [3], Swanner Elizabeth D. [4], Li Yi-Liang [5], Crowe Sean A. [6, 7], Planavsky Noah J. [8], Reinhard Christopher T. [9], Lalonde Stefan [10]

[1] Univ Alberta, Dept Earth & Atmospher Sci, Edmonton, AB T6G 2E3, Canada.
[2] Albert Ludwigs Univ, Inst Geo & Umweltnat Wissensch, Mineral Geochem, D-79104 Freiburg, Germany.
[3] Univ Tubingen, Dept Geomicrobiol, Ctr Appl Geosci, D-72074 Tubingen, Germany.
[4] Iowa State Univ, Dept Geol & Atmospher Sci, Ames, IA 50011 USA.
[5] Univ Hong Kong, Dept Earth Sci, Pokfulam Rd, Hong Kong, Hong Kong, Peoples R China.
[6] Univ British Columbia, Dept Microbiol & Immunol, Vancouver, BC V6T 1Z4, Canada.
[7] Univ British Columbia, Dept Earth Ocean & Atmospher Sci, Vancouver, BC V6T 1Z4, Canada.
[8] Yale Univ, Dept Geol & Geophys, POB 6666, New Haven, CT 06511 USA.
[9] Georgia Inst Technol, Sch Earth & Atmospher Sci, Atlanta, GA 30332 USA.
[10] European Inst Marine Studies, CNRS UMR6538, Lab Domaines Ocean, Technopole Brest Iroise, F-29280 Plouzane, France.

* Corresponding author : Kurt O. Konhauser, email address : kurtk@ualberta.ca

Abstract :

Banded iron formations are economically important sedimentary deposits in Earth's Precambrian rock record, consisting of alternating iron-rich (hematite, magnetite, and siderite) and silicate/carbonate (quartz, claylike minerals, dolomite, and ankerite) layers. Based on chemical analyses from banded iron formation units of the 2.48 Ga Dales Gorge Member of the Hamersley Group in Western Australia, it has been previously suggested that most, if not all, of the iron in banded iron formations could have been oxidized by anoxygenic phototrophic bacteria (photoferrotrophs) at cell densities considerably less than those found in modern iron-rich aqueous environments. However, oxygen-producing phytoplankton may have also been capable of supplying the necessary oxidizing power. Here, we revisit the question of the anoxygenic and oxygenic phytoplankton populations necessary to account for banded iron formation deposition and quantify the amount of selected trace elements (P, Mn, Co, Ni, Cu, Zn, Mo, Cd) that could have been associated with their biomass. Using an expanded geochemical data set for the Dales Gorge Member as an example, we find that with turnover times comparable to those seen in modern ecosystems, the same phytoplankton populations required to form banded iron formations could have supplied the entirety of trace elements found in this iron-rich deposit. Further, spurred by the similarities between banded iron formation and anoxygenic phytoplankton trace-element stoichiometries, we suggest that much of the trace-element inventory preserved in the banded iron formation was at some point biologically assimilated in the water column, released from degrading photoferrotrophic biomass at the seafloor and in the sediment pile, and ultimately fixed in the iron-rich sediment in approximately stoichiometric

proportions by near-quantitative adsorption to ferrihydrite. Our observations suggest that, as today, phytoplankton and the recycling of their biomass exerted control over the trace-element composition of ancient seawater and sediment.

INTRODUCTION

It is widely accepted that during the Precambrian, photosynthetic planktonic bacteria were involved in the oxidation of dissolved Fe(II) and the resultant precipitation of Fe(III) that led to BIF deposition (see Köhler et al., 2010; Posth et al., 2013 for reviews). Two possible roles are envisioned. The first is predicated on the presence of ancient cyanobacteria (e.g., Cloud, 1973) that produced oxygen that reacted with dissolved Fe(II) to form ferric oxyhydroxide phases (e.g., Chan et al., 2016) such as ferrihydrite ($Fe[OH]_3$), the likely precursor sediment to BIF (see Bekker et al., 2014). These oxygenic phototrophs would have flourished whenever bioessential trace elements were available, creating "oxygen oases" in the upper water column (Olsen et al., 2013; Swanner et al., 2015), perhaps as early

as 3.0 Ga (Planavsky et al., 2014), if not earlier (see Satkoski et al., 2015; Frei et al., 2016). The second, and arguably the more ancient role, is ascribed to anoxygenic photosynthetic bacteria that used Fe(II) as a reductant for CO_2 fixation (e.g., Garrels and Perry, 1974; Ehrenreich and Widdel, 1994). Although the Fe(II) oxidation rate of these photoferrotrophs is dependent upon light intensity, they can grow in low light regimes befitting the deeper marine photic zones (e.g., Biebl and Pfenning, 1978; Crowe et al., 2008); it has been estimated that sufficient light for their metabolism could penetrate up to 100 m ocean depth (Kappler et al., 2005). Therefore, these microorganisms could easily have oxidized all the upwelling Fe(II) before it met oxygenated surface waters (if these existed) in Archean oceans. Moreover, Jones et al. (2015) recently suggested that photoferrotrophs could also have exhausted dissolved phosphorous in upwelling waters, depriving cyanobacteria in overlying waters of this key nutrient.

Over a decade ago, Konhauser et al. (2002) calculated that for a major BIF deposit, such as the 2.48 Ga Dales Gorge Member of the Brockman Iron Formation, Hamersley Group, Western Australia, on average 4.53×10^{12} moles of Fe (or 45.3 mol m^{-2} when normalized to a surface area of 10^{11} m^2) were precipitated annually during periods of peak ferric iron deposition. This sedimentation rate would have required some 5.0×10^{23} cells of either photoferrotrophic (e.g., *Chromatium* sp.) or microaerophilic, chemolithoautotrophic, Fe(II)-oxidizing bacteria (e.g., *Gallionella* sp.) per year. Assuming that Fe(II) oxidation was restricted to the upper 100 meters of the water column, then a minimum cell density of $\sim 5 \times 10^4$ cells ml^{-1} would have been required to precipitate an annual BIF layer (Konhauser et al., 2002). Once the anoxygenic or oxygenic phytoplankton died, some of the cellular remains would have settled through the water column with ferrihydrite particles and been deposited at the seafloor as the precursor sediment to BIF. These biomass-ferrihydrite aggregates then served as a substrate for bacteria performing dissimilatory Fe(III) reduction (DIR) within the sediments, leading to the oxidation (and loss) of organic carbon, as well as the early diagenetic

85 precipitation of Fe(II)-bearing minerals such as magnetite (Fe_3O_4) and siderite ($FeCO_3$) (e.g.,
86 Konhauser et al., 2005; Heimann et al., 2010; Li et al., 2011; Köhler et al., 2013). At the time,
87 Konhauser et al. (2002) speculated that those sedimenting ferrihydrite particles would have
88 transported trace elements to the seafloor along with the decaying biomass. However, several recent
89 studies have since suggested that in the Precambrian oceans, those same minerals may not have been
90 as reactive as previously believed because dissolved silica (e.g., Konhauser et al., 2007a; 2009) and
91 organic carbon (Eickhoff et al., 2014) passivates the surface reactivity of ferrihydrite towards other
92 ions.

93 It is also possible that the biomass itself may have been a major contributor to the trace element
94 inventory of BIF. Li et al. (2011) suggested that phytoplankton may have played a key role in the
95 transfer of phosphorous (via intracellular assimilation) from the photic zone to the seafloor. It is also
96 likely that the high surface reactivity of marine phytoplankton (e.g., Sañudo-Wilhelmy et al., 2004;
97 Dittrich and Sibler, 2005; Hadjoudja et al., 2010) could similarly have adsorbed cationic trace metals,
98 and ultimately facilitated their deposition into marine sediments such as BIF. Indeed, Martinez et al.
99 (2016) recently applied surface complexation modelling (SCM) to describe trace metal cation
100 sorption to one of the two marine photoferrotrophs isolated to date, *Rhodovulum iodosum* (the other
101 being *Rhodovulum robiginosum*; Straub et al., 1999), and calculated that the trace metal inventory
102 (i.e., Mn, Co, Cu, Zn, Ni and Cd) in 3.75 Ga BIF in the Nuvvuagittuq Supracrustal Belt in Quebec,
103 Canada, could entirely be accounted for by adsorption onto bacterial surface functional groups at
104 ocean-relevant aqueous conditions. Importantly, Hao et al. (2013) and Martinez et al. (2016) also
105 determined that in the composites of ferrihydrite, intact cells, and extracellular polysaccharides (EPS)
106 that photoferrotrophs produce, the surface functional groups responsible for most of the metal cation
107 adsorption were those corresponding to the organic matter fraction. This is consistent with the results
108 of previous studies of bacteriogenic iron oxide surface reactivity, where the surface charge of such

109 organic-mineral composites was dominated by contributions from reactive groups associated with the
110 bacterial cell fraction (Mikutta et al., 2012; Moon and Peacock, 2013). Similarly, Liu et al. (2015)
111 evaluated Cd adsorption onto the marine cyanobacterium *Synechococcus* sp. PCC 7002, and
112 demonstrated that an active bloom with 10^4-10^5 cells/mL at pH 8 could adsorb 1-10 nmol of Cd per
113 liter of seawater. Indeed, at a total Cd in modern seawater of 8 nM (e.g., Pai and Chen, 1994), a
114 population of *Synechococcus* could theoretically adsorb effectively all dissolved Cd from seawater in
115 the photic zone if equilibrium metal adsorption conditions were achieved. Of course, near complete
116 Cd adsorption to marine biomass is not observed due to competing adsorption reactions as well as
117 aqueous Cd complexation in seawater by chloride (predominantly as $CdCl_2^0$ and $CdCl^+$; Bryne et al.,
118 1988) and by organic ligands (Bruland, 1992), all of which act to reduce the concentration of free
119 aqueous Cd^{2+} available to adsorb to cell surface functional groups.

120 In this study, we revisit the quantity of trace elements supplied by biomass to BIF. We first
121 estimate the amount of ferric iron deposited in an annual layer, and in turn, the amount of trace
122 elements deposited annually, using literature and new geochemical data obtained for the Dales Gorge
123 Member. For photoferrotrophic biomass, refined surface adsorption models have recently become
124 available (Martinez et al., 2016) which allow for an evaluation of the amount of trace elements that
125 could have been sequestered through adsorption. To date, high-quality trace element assimilation data
126 for photoferrotrophs are lacking, and in this regard, we have performed a series of experiments to
127 provide per-cell metal loadings associated with their biomass. As a comparison, we also consider per-
128 cell metal loadings associated with metal assimilation by oxygen-evolving cyanobacterial and
129 eukaryotic phytoplankton. The expected flux of trace metals from these different biomass sources to
130 BIF is then evaluated in light of both the number of phytoplankton cells implicated in BIF deposition
131 (i.e., only enough cells to form BIF), as well more realistic cell numbers when modern turnover rates
132 are considered, in order to understand their contribution to BIF trace element inventories.

METHODS

BIF trace metal analyses

To assess the importance of biomass as a trace metal shuttle to BIF sediment, we first assembled an expanded trace metal dataset for the 2.5 Ga Dales Gorge Member, the BIF from which Konhauser et al. (2002) made the initial calculations of how many bacteria were required annually to precipitate the ferric iron component in BIF. Data were sourced from literature as well as new geochemical analyses of drill core samples (Table S1). In this work, we focused on oxide-facies BIF samples (rich in hematite- and magnetite; c.f. James, 1954) because it is generally presumed that they formed via dehydration and/or partial reduction of a precursor ferrihydrite phase (Ewers and Morris, 1981; Han et al., 1988; Ahn and Buseck, 1990; Krapež et al., 2003; Bekker et al., 2010), and thus contains the most 'primary' iron minerals in BIF (Sun et al., 2015). This view is consistent with Fe isotope systematics, which require iron oxide delivery to the sediment water interface (e.g., Johnson et al., 2008; Planavsky et al., 2012). For an alternative interpretation proposing that greenalite [$(Fe)_3Si_2O_5(OH)_4$] was the primary phase, and was oxidized by oxygen-bearing meteoric waters sometime after 2.2 Ga, see Rasmussen et al. (2015, 2016, 2017).

For new trace element analyses performed for this study, samples were cut into slabs and broken into small chips (<5 mm) without metal contact, and between 20 and 150 g were powdered in an automated agate mill. Approximately 50 mg of crushed rock powder (<100 mesh) was digested sequentially in a class 1000 clean lab at IFREMER (Centre de Brest, France) in PFA vials at 90ºC using concentrated HF-HNO_3, aqua regia, and 6M HCl. Aliquots were resuspended in 2% HNO_3 with indium as an internal standard and analysed for trace element concentrations using a Thermo Scientific Element2 High Resolution Inductively Coupled Plasma Mass Spectrometer at the Pôle Spectrométrie Océan in Brest, France. The instrument was calibrated with multi-element solutions and the results verified against geostandards BHVO-2, IF-G, and GL-O treated in the same batch.

Precisions based on the repeated analysis of standards, expressed as 2 relative standard deviations (RSD), ranged from <3% for rare earth elements analyzed in low resolution to 4-8% for transition metals analyzed in medium resolution.

Growth of Rhodovulum iodosum

The basal salts and $NaHCO_3$ of marine phototroph (MP) medium for the cultivation of *R. iodosum* were prepared according to the protocol described by Wu et al. (2014). Sterile additions made after autoclaving included 3 mg L^{-1} filtered $FeCl_3$, a selenium and tungstate solution (0.4 g NaOH, 6 mg $Na_2SeO_3 \cdot 5H_2O$, and 8 mg $Na_2WO_4 \cdot 2H_2O$ in 1 L Millipore water), 0.5 mM $Na_2S_2O_3$, and 1 ml each of a vitamin and trace element solution. For the trace element solution, 5 mL of 25% HCl were added to 495 ml ultrapure water containing 2.86 g L^{-1} H_3BO_3, 0.5 g L^{-1} $MnCl_2 \cdot 4H_2O$, 24 mg L^{-1} $NiCl_2 \cdot 6H_2O$, 190 mg L^{-1} $CoCl_2 \cdot 6H_2O$, 180 mg L^{-1} $ZnCl_2$, 36 mg L^{-1} $Na_2MoO_4 \cdot 2H_2O$, 2 mg L^{-1} $CuCl_2 \cdot 2H_2O$, and a final concentration of 7.5 mM Fe(II) added from an oxidized elemental Fe solution to eliminate trace metal contamination from an Fe(II) salt. The elemental Fe was washed with acetone to remove organic contaminants, then dissolved and oxidized to Fe(II) in anoxic 1 N HCl in a glovebox (100% N_2). The vitamin solution contained 10 mg L^{-1} D(+)-biotin, 50 mg L^{-1} vitamin B_1, 250 mg L^{-1} vitamin B_6, 50 mg L^{-1} aminobenzoic acid, 25 mg L^{-1} D-pantothenic acid, 100 mg L^{-1} nicotinic acid, and1 g L^{-1} vitamin B_{12}, and was omitted in cobalt-limiting experiments. The pH of the medium was adjusted to 6.8 using 1 N HCl or 0.5 M Na_2CO_3 as described in Hegler et al. (2008). To determine how the photoferrotrophs respond to varying concentrations of metals, we varied the amount of metal in the medium by adding trace element solutions representing 0.5X, 1X, 2X, and 5X the metal concentrations in the basal (1X) medium. The concentration of metals in the 1X medium was as follows (in μM): V (0.03), Mn (2.30), Co (1.2), Ni (0.23), Cu (0.05), Zn (2.42), Mo (0.27), and Cd (0.00007).

Media (100 mL) was dispensed into 200 mL borosilicate glass bottles and sealed with butyl rubber stoppers to maintain anoxic conditions. All glassware was of borosilicate composition, and was acid-washed in 1N HCl for 24 hours, then soaked in ultrapure water (conductivity 0.0555 μS) for at least 48 hours, then rinsed with fresh ultrapure water to remove adsorbed metals. Butyl rubber stoppers were acid-washed in 1N HCl for 24 hours, and then boiled three times in ultrapure water.

Experiments were inoculated to 1% (v/v) with a log-phase culture. All experiments were conducted in triplicate. Cultures of *R. iodosum* were incubated at a constant intensity of 12.82 μmol photons m^{-1} s^{-1} from a standard 40W tungsten light bulb at 24°C under static conditions. Because H_2 was the electron donor for photosynthesis, H_2:CO_2 (80:20) gas was flushed through the headspace every 2-3 days.

Metal Assimilation by Rhodovulum iodosum

The concentrations of all metals in trace element and vitamin solutions were determined using a ICP-OES (Perkin Elmer Optima 5300 or Horiba Ultima 2) or ICP-MS (Thermo Scientific Element2). Certified commercial multi-element standards were used for calibration. Liquid samples of all media depleted in metals were analyzed in triplicate. To determine the concentration of metals in the cytoplasm, cells were harvested in the stationary phase by centrifugation and the pellet washed three times in 0.01 N HCl to remove adsorbed metals from the cell surface. The cells were freeze-dried and then digested in concentrated trace metal grade HNO_3 at 60°C in acid-washed PFA vials. The residues were resuspended in 8 M HNO_3 and further diluted in 2% HNO_3 before analysis.

The concentrations of metals in dried biomass were used to determine the cellular metal quotas (Q_{Me}; μmoles L^{-1}) present in cells of each strain under different conditions. The number of cells per liter was determined after establishing a standard curve relating OD_{660} measurements to fluorescent cell counts (Wu et al., 2014). Then, a suspension of a known cell density was dried and weighed to determine the dried biomass weight.

Modelling bacterial surface reactivity to various divalent cations

Martinez et al. (2016) recently investigated the surface proton reactivity of a *R. iodosum*-ferrihydrite composite, and calculated protonation constants (pKa's) and corresponding site densities. Using the protonation model of Martinez et al. (2016), we employed a free linear energy approach to extrapolate metal-organic binding constants from metal-acetate complexes (constants from Martell and Smith, 1977) to cell surface carboxyl groups (c.f., Fein et al., 2001; Martinez et al., 2016). This is justified as carboxyl groups are the dominant deprotonated sites for metal adsorption at marine pH values, and bacteria have been repeatedly shown to exhibit broadly similar metal binding behaviour across species (e.g., Yee and Fein, 2001; Borrok et al., 2004a; 2004b). We employed a modern seawater pH of 8 for all adsorption calculations, consistent with previously predicted ranges for Paleoproterozoic seawater (e.g., 5.7-8.3, Grotzinger and Kasting, 1993; 7.7-8.3, Tosca et al., 2015; and 6.7-7.8 Blättler et al., 2016). Additional constraints include *R. iodosum* cell densities of 1.9 x 10^4 cells/mL (see below), and an initial trace metal composition equivalent to modern mean seawater after Bruland and Lohan (2003).

To calculate the removal of trace metals from seawater to *R. iodosum* surface functional groups, we first determined the number of deprotonated ligands at pH 8 using the Martinez et al. (2016) protonation model. Then, using metal binding constants calculated as described above, we calculated the concentration of metal removed from solution, for each metal individually. The concentration of deprotonated bacterial surface sites (mol sites per L seawater), was nearly three times greater than the sum concentration of all trace metals of interest. Following adsorption, only a miniscule fraction, well under 0.1%, of the total deprotonated sites, are occupied by the tested metals. For this reason, a model that considers the simultaneous competition of all tested metals for adsorption to *R. iodosum* surface sites was deemed unnecessary.

Model runs were performed for three versions of seawater, one with a modern composition (after Bruland and Lohan, 2003), one simulating the composition of seawater during deposition of the 2.48 Ga Dales Gorge Member, and one stoichiometrically fixed to *R. iodosum* and 9 nM Ni (Table S2). Simulated Paleoproterozoic seawater was set at 10 nM Co, 3 nM Cu, 400 nM Ni, 10 nM Zn, and 0.6 nM Cd, and was based on upper estimates for several trace metals to test conditions under which the greatest extent of metal competition and adsorption is expected. Estimates were derived from empirical rock record constraints when possible (Ni^{2+}, Zn^{2+}), or from thermodynamic solubility limits when those were unavailable (Mn^{2+}). Zn^{2+} was set at 10 nM based on Robbins et al. (2013) and Scott et al. (2013), and similarly, Ni^{2+} was set at 400 nM Konhauser et al. (2009; 2015). For Cu^{2+}, a modern concentration was assumed as the geological record shows little variation (Fru et al., 2016). Manganese was increased above modern values based on the estimates of Saito et al. (2003). Finally, Co^{2+} was set at a higher concentration than modern based on Saito et al. (2003) and Swanner et al. (2014). For a lack of strong empirical constraints, Cd^{2+} concentrations were maintained at modern concentrations.

Modelling Metal Adsorption by Ferrihydrite

The adsorption of trace metals to ferrihydrite was modelled using the chemical speciation software visual MINTEQ (Gustafsson, 2013) using the hydrous ferric oxide (HFO) surface complexation model of Dzombak and Morel (1990) that is built into the visual MINTEQ package. This model invokes two amphoteric functional groups at the HFO surface to account for proton and metal adsorption and a diffuse double layer to account for the electrostatic field that develops as a function of pH at the HFO surface. Modelling conditions were 25ºC with a matrix of 0.56 M NaCl. Metals were allowed to simultaneously compete for adsorption onto surface sites, and we accounted for the impacts of major hydroxide, carbonate, and chloride aqueous complexes with the metals of interest. To evaluate how trace elements released from decaying biomass may be fractionated during

adsorption to ferrihydrite, adsorption was calculated using the trace metal composition of simulated seawater with the trace metals under consideration fixed to phototrophic assimilated proportions, anchored around fixed Ni concentration of 9 nM, similar to modern seawater and conservatively below estimates for Paleoproterozoic seawater ca. 2.5 Ga (Konhauser et al., 2009; Table S2; see below).

RESULTS AND DISCUSSION

The amount of trace elements in an annual BIF layer

In Konhauser et al. (2002), the authors purposefully used a sedimentation rate of 1 mm yr^{-1} hematite equivalent (assuming ~95% compaction, the actual wet sediment deposition rate would have been much higher; Trendall and Blockley, 1970) throughout the Hamersley Basin (10^{11} m^2) to emphasize that even under unrealistically rapid sedimentation rates, marine bacteria could have precipitated all the ferric iron in the Dales Gorge Member BIF. In this study, we conservatively apply lower sedimentation rates of ferrihydrite based on a proposed modern analogue for BIF deposition, the ferruginous Lake Matano in Indonesia (Crowe et al., 2008, 2011). Recently, Kuntz et al. (2015) determined an annual Fe(III) burial rate of 0.35 mmol m^{-2} day^{-1}, or around 0.3 mm yr^{-1}, assuming a sediment water content of 80% by mass. Furthermore, based on a presumed initial deposit for BIF of 80% $Fe(OH)_3$ and 20% amorphous SiO_2 (which is now manifest as Fe-rich mesobands in oxide-type BIF containing approximately 80% hematite/magnetite and 20% quartz; Konhauser et al., 2002), with corresponding densities of 3.8 g cm^{-3} and 2.2 g cm^{-3}, respectively, yielding a total density of 3.48 x 10^6 g m^{-3}, the annual Dales Gorge BIF mass was 1.04 x 10^{11} kg for a 0.3 mm sedimentation rate over the entire depositional area of 10^{11} m^2. We further note that assuming a 20% initial silica component to the sedimenting ferrihydrite particles is consistent with recent studies that have suggested that the

primary Fe(III) precipitate in BIF was an Fe(III)-silica gel (Percak-Dennett et al., 2011; Reddy et al., 2016; Zheng et al., 2016)

Based on geochemical analyses of oxide-facies BIF in the Dales Gorge Member (Alibert and McCulloch, 1993; Pecoits et al., 2009; Konhauser et al., 2009; 2011, as well as new analyses performed for this study; see Table S1), we calculate an average concentration (in mg kg^{-1}) for P (941.0), Zn (17.9), Co (3.9), Cu (5.7), Ni (10.1), Mo (1.4), Cd (1.2) and Mn (240.0). Using the annual mass calculated above, this is readily translated into an average annual flux (in moles; see Table 1A) of P (3.17×10^9), Zn (2.85×10^7), Co (6.96×10^6), Cu (9.33×10^6), Ni (1.80×10^7), Mo (1.48×10^6), Cd (1.09×10^6), and Mn (4.56×10^8).

The number of cells required to form an annual BIF layer

Peak iron deposition in the Dales Gorge Member is estimated at 4.38×10^{13} g or 7.85×10^{11} mol of Fe $year^{-1}$ (based on the mass calculation of 1.04×10^{11} kg and an average Fe_{TOTAL} of 42 wt. % for the precursor sediments). For oxygen-evolving phytoplankton (e.g., cyanobacteria) to have been responsible for Fe(II) oxidation (using $12Fe^{2+} + 3O_2 + 30H_2O \rightarrow 12Fe(OH)_3 + 24H^+$), a net oxygen production rate of approximately 1.96×10^{11} mol O_2 $year^{-1}$ would have been needed. For a depositional basin for the Dales Gorge Member of 10^{11} m^2, this translates to a depth-integrated production rate of 5.37 mmol O_2 m^{-2} day^{-1}. Depth-integrated net oxygen production rates in modern ocean regions generally range from slightly below zero (net heterotrophic; Arabian Sea, N.C. Pacific Gyre) to 10–40 mmol O_2 m^{-2} day^{-1} (N.E. Atlantic, Mediterranean Sea, Baltic Sea), with highly productive regions like the Southern Ocean reaching up to ~110 mmol O_2 m^{-2} day^{-1} (Williams, 1998). Cyanobacteria in the Hamersley Basin photic zone would thus need to achieve net O_2 production rates that are at the lower end of what is observed today. Assuming a 100-meter photic zone and a cyanobacteria cell-specific O_2 production rate of 50 fmol $cell^{-1}$ $hour^{-1}$ (Tang et al., 2014), this translates to a total population of 4.5×10^{20} cells, or only ~45 cells ml^{-1}, needed to form BIF. This

297 cell density is unrealistically low considering that it assumes a maximal rate of oxygen production
298 under optimal light and nutrient conditions in culture (Tang et al., 2014), but is important nonetheless
299 in that it quantitatively demonstrates for the first time that relatively small populations of
300 cyanobacteria could readily have generated the oxidizing equivalents required for BIF deposition.
301 Interestingly, the modest depth-integrated O_2 production rate required to oxidize the Fe(II) in the
302 Dales Gorge Member (5.37 mmol O_2 m^{-2} day^{-1}) means that even muted photic zone O_2 production
303 (by modern standards) would have had the effect of completely scrubbing dissolved Fe(II) from
304 seawater, such that the upper photic zone in the Paleoproterozoic (and thereafter) would have had
305 essentially no dissolved Fe(II).

306 In the case of photoferrotrophy, instead of using the cell densities from Konhauser et al.
307 (2002), who calculated the cell number-normalized Fe(II) oxidation rates for the freshwater
308 *Chromatium* sp. strain L7 (as per Ehrenreich and Widdel, 1994), we use here the recently determined
309 Fe(II) oxidation rates for the marine strain *R. iodosum*. Based on reported Fe(II) oxidation rates of
310 0.15 mM Fe(II) day^{-1} at 0.43 mM Fe(II), a light intensity of 12 μmol quanta m^{-2} s^{-1}, and a cell density
311 of 2.3 x 10^8 cells ml^{-1} during log phase at 240 hours, Wu et al. (2014) calculated that each individual
312 cell (taking day-night light cycles into consideration) can oxidize 4.11 x 10^{-12} moles Fe(II) $year^{-1}$. At
313 an annual precipitation rate of 7.85 x 10^{11} mol of Fe, approximately 1.91 x 10^{23} metabolizing cells of
314 *R. iodosum* would be required to precipitate an annual BIF layer. Taking the same depositional basin
315 area and 100 m photic zone as above, this yields a minimum cell density of 1.91 x 10^4 cells ml^{-1}. This
316 is approximately 1/3 of the cell density required by the calculations of Konhauser et al. (2002) for
317 BIF deposition (having then assumed 1 mm yr^{-1} deposition of hematite) by *Chromatium* sp. strain L7,
318 effectively validating those earlier calculations with data from a second strain. The importance of
319 these calculations is that the cell densities necessary to precipitate the ferric iron in BIF are

considerably less than modern populations of bacterial phytoplankton growing in the photic zone of modern marine coastal waters (10^4–10^6 cells ml^{-1}; Miyazono et al., 1992; Jacquet et al., 1998).

We emphasize that the above calculations correspond to the minimum number of cells required to precipitate BIF, not the maximum carrying capacity of the water column. They also disregard cell turnover, which is an important factor when considering the total amounts of metals that would have been associated with sinking biomass over the course of BIF deposition (see below). Finally, these calculations ignore the possibility of alternative oxidation mechanisms such as UV photo-oxidation or atmosphere-derived oxidants such as hydrogen peroxide. Several studies suggest these mechanisms are of less importance than the biological oxidation mechanisms we explore here (e.g., Konhauser et al., 2007b; Pecoits et al., 2015).

Potential contributions from trace elements assimilated by photoferrotrophic biomass

In terms of trace element assimilation, we determined that a population of *R. iodosum* cells at stationary phase incorporated from the 1X medium the following (average in $\mu g\ g^{-1}$); P (2.6×10^4), Zn (3.5×10^2), Co (3.1×10^1), Cu (2.0×10^1), Ni (3.6×10^1), Mo (4.8), and Cd (0.02), and Mn (4.5×10^1). Growth rates for *R. iodosum* did not change significantly between the 1X and 0.5X, 2X or 5X metals medium (Table S3). Biomass yields were significantly higher in the 0.5X medium as compared to 1X, and lower in the 5X medium as compared to 1X, while the range of intracellular metal concentrations varied little despite changes in the medium composition.

Although elemental variability naturally occurs between species as a function of growth rate and in response to ambient nutrient concentrations in seawater (Bruland et al., 1991; Twinning et al., 2004), and that ancestral photoferrotrophs may have behaved differently, the intracellular metal concentrations we determined for *R. iodosum* provide a basis for examining the magnitude by which phytoplankton may assimilate trace elements from seawater. To start, we first estimate the mass of an individual *R. iodosum* cell as follows: with an average *R. iodosum* cell volume of 1.5 μm^3 (Straub

et al., 1999), and a proportionate mass to *Gallionella* (where each cell has a volume of ~1 μm^3 and has a wet mass of 1×10^{-12} g; Hallbeck and Pedersen, 1991), an individual *R. iodosum* cell is 1.5 x 10^{-12} g $cell^{-1}$. Then, using our elemental stoichiometry from above, we calculate the mass of trace elements assimilated by a *R. iodosum* cell, which, multiplied by a total cell population of 1.91 x 10^{23} cells, yields an annual quantity assimilated (in moles) for the entire 100 m-deep photic zone for P (2.40 x 10^8), Zn (1.54 x 10^6), Co (1.50 x 10^5), Cu (9.07 x 10^4), Ni (1.77 x 10^5), Mo (1.43 x 10^4), Cd (5.10 x 10^1), and Mn (2.37x 10^5) (Table 1B).

The quantity of trace elements adsorbed by R. iodosum

Using the calculated sorption values for *R. iodosum* (methods above; Table S4), we calculated the amounts of metal adsorbed for modern mean seawater concentrations (Burland and Lohan, 2003) at pH 8 (in μmol of metal mg^{-1}) as follows: Zn (5.03 x 10^{-6}), Co (2.01 x 10^{-8}), Cu (2.73 x 10^{-5}), Ni (2.72 x 10^{-6}), Cd (2.42 x 10^{-6}), and Mn (1.22 x 10^{-7}). For a photoferrotroph population of 1.91 x 10^{23} cells, at an estimated 1.5 x 10^{-12} g $cell^{-1}$, this equates to annual fluxes due to biomass sorption (in moles): Zn (1.44 x 10^3), Co (5.77 x 10^0), Cu (7.82 x 10^3), Ni (7.79 x 10^2), Cd (6.93 x 10^2), and Mn (3.50 x 10^1) (see Table 1C). Importantly, for most elements analyzed, we calculate that intracellular assimilation of metals accounts for between one to four orders of magnitude more metal than does adsorption to surface functional groups at seawater conditions (Table 1D). Accordingly, we consider assimilation to be the more important mechanism for the concentration of metals by *R. iodosum* biomass. Cd, which is a notable exception, likely has a more restricted role in metalloenzymes (e.g., Price and Morel, 1990); metal adsorption to bacterial surfaces is predicted to account for over 90% of the overall Cd uptake.

To test the sensitivity of the *R. iodosum* adsorption model to variations in initial seawater compositions, several iterations were run for three different seawaters conditions (Tables S2, S4).

Although, as expected when initial seawater concentrations are greater (i.e., for a simulated Paleoproterozoic seawater or seawater stoichiometrically fixed to *R. iodosum*), there is a greater amount of trace metals adsorbed to the surface of *R. iodosum*. Critically, however, for each of the three seawater conditions considered assimilation remains at least an order of magnitude greater than adsorption for all elements considered here except Cd as discussed above (data not shown). This suggests that the metal fluxes calculated here are reliant upon bacterial trace metal assimilation rather than surface adsorption, and are thus relatively insensitive to minor shifts in the trace metal composition of seawater or small changes in pH (see supplementary information).

Trace element assimilation by other phytoplankton and potential biomass contributions to BIF

To put our work into context, we further compare the molar stoichiometry of metals assimilated by *R. iodosum*, as normalized to P:

$$P_{1000}Mn_{0.99}Co_{0.62}Ni_{0.74}Cu_{0.38}Zn_{6.42}Mo_{0.06}Cd_{0.0002}$$

with the molar stoichiometry reported for natural marine cyanobacteria (lithogenic-corrected values from Walve et al., 2014 and data from references therein):

$$P_{1000}Mn_{1.26}Co_{0.02}Ni_{1.94}Cu_{0.42}Zn_{1.65}Mo_{0.49}Cd_{0.007}$$

as well as with the average stoichiometry for 15 marine eukaryotes (excluding the hard parts, using the volume-normalized average of Ho et al., 2003; Ni is unavailable):

$$P_{1000}Mn_{3.5}Co_{0.20}Cu_{0.29}Zn_{0.67}Mo_{0.03}Cd_{0.14}$$

While we consider it unlikely that eukaryotic phytoplankton contributed to BIF deposition during the Paleoproterozoic, we include them nonetheless to cover the range of photosynthetic biomass that might drive Fe(II) oxidation. For simplicity, we assume a cellular volume of 100 μm^3 to calculate cell-specific trace element loadings; in reality the volumes can range from as low as 10 μm^3 for the green alga *Pycnococcus provasoli* to 7000 μm^3 for the diatom *Ditylum brightwellii* (Ho et al.,

2003). Further, we acknowledge that phytoplankton C:P ratios and C:Zn ratios can vary widely, especially in cyanobacteria (e.g., Twining et al., 2004; Nuester et al., 2012; Reinhard et al., 2017). This variability will change the ratio of ferric iron to organic matter produced, but it will not change phytoplankton P to trace metal ratios. Given that the evolution of phytoplankton C:P ratios are difficult to estimate (Planavsky, 2016; Reinhard et al., 2017) this adds some uncertainty to but does not undermine our approach.

Using the average cellular volume provided by Ho et al. (2003), and the same population of eukaryotic cells as cyanobacteria needed to produce the O_2 for annual BIF deposition (4.5×10^{20} cells), yields an annual flux (in moles) of biomass-assimilated P (5.40×10^{6}), Zn (3.60×10^{3}), Co (1.08×10^{3}), Cu (1.58×10^{3}), Mo (1.40×10^{2}), Cd (7.65×10^{2}), and Mn (1.89×10^{4}) (see Table S5). For cyanobacteria, using the same cell population, we calculate annual biomass contributions via assimilation as follows: P (6.78×10^{4}), Zn (1.12×10^{2}), Co (1.47×10^{0}), Cu (2.86×10^{1}), Ni (1.31×10^{2}), Mo (3.32×10^{1}), Cd (4.86×10^{1}), and Mn (8.55×10^{1}) (see Table 1E).

Considering cell populations implicated for BIF deposition by photoferrotrophic bacteria (1.9×10^{23} cells) or by cyanobacteria (4.5×10^{20} cells), we then use these cell-specific trace element loadings to explore the trace metal fluxes that biomass may have supplied to BIF on an annual basis. Biomass–associated trace element fluxes are presented in Figure 1A alongside average trace element fluxes implied for the Dales Gorge Member, as determined from a compilation of between 40 and 240 independent samples per trace element analysed (c.f. Table S1). Assimilated trace metals associated with cyanobacteria and eukaryotes share some similarities, and for simplicity, trace metals that would have been associated with a eukaryotic population are not shown. It is immediately clear that for the minimum cell populations required for BIF deposition, sinking biomass cannot account for the entirety of the annual Dales Gorge Member exit flux of trace elements. In the case of *R.*

413 *iodosum*, the calculated biomass falls short in P (by a factor of 13, i.e., 1/0.0758), Zn (18), Co (46),
414 Cu (95), Ni (101), Mo (104), Cd (1467), and Mn (1922), (Table 1D).

415 However, it is important to note that these calculations assume that the minimum number of
416 cells required to form the Dales Gorge Member experienced no turnover. In other words, the
417 calculation of 1.91 x 10^{23} metabolizing cells of *R. iodosum* required to precipitate an annual BIF layer
418 assumes that each individual cell oxidized dissolved Fe(II) for an entire year, which would not be the
419 case. Indeed, as today, the population of marine phytoplankton in Paleoproterozoic surface waters
420 was likely dynamic, with new growth occurring in lockstep with cell death to maintain a roughly
421 stable population size. Doubling times of marine cyanobacteria are on the order of days, as fast as
422 three days in culture under optimum conditions (Capone et al., 1997). Photoferrotrophs in culture
423 show a similar range of doubling times (1–4 days; Wu et al., 2014). Assuming a three-day doubling
424 time, the entire population of cells would have been renewed ~121 times over the course of a year.
425 This would have led to 2.31 x 10^{25} metabolizing cells yr^{-1}, and each with its own trace element-laden
426 biomass. Under these conditions, the amount of trace elements that would have cycled annually
427 through a dynamic population of photoferrotrophs maintaining the minimum cell population required
428 for deposition of the Dales Gorge Member corresponds to the entirety of the trace elements preserved
429 therein (Figure 1A). By contrast, trace element contributions from the marine cyanobacterial
430 population required to form the BIF fail to meet the observed BIF exit fluxes even with a 3-day
431 doubling time (estimated at 5.45 x 10^{22} metabolizing cells), the highest observed in culture (Figure
432 1A).

433 We also calculated trace element fluxes that would have been associated with detrital
434 contributions to the Dales Gorge Member (based on average Ti concentrations in the BIF and
435 assuming trace element/Ti ratios corresponding to average continental crust; Table S6), as well as
436 hydrothermal fluxes to the Hamersley basin photic zone (based on global hydrothermal inputs to

437 seawater; Table S6). With the exception of Mn, which like Fe has a strong hydrothermal source,
438 neither detrital material nor hydrothermal fluids appear to have been important in determining the
439 trace element composition of BIF for the elements considered in this study. Furthermore, irrespective
440 of how trace elements may have been supplied to seawater, our calculations show that the entire BIF
441 inventory should have been cycled through biomass before being ultimately buried in BIF.

442 ***Trace element contributions from ferrihydrite to BIF***

443 Several previous studies have considered the role that the sedimenting ferrihydrite particles played in
444 the transfer of trace elements from the water column to the seafloor where BIF accumulated (e.g.,
445 Bjerrum and Canfield, 2002; Konhauser et al., 2009; Jones et al., 2015). To better understand this
446 contribution, we used a surface protonation model for pure ferrihydrite and the metal binding
447 constants of Dzombak and Morel (1990) to examine the extent of adsorption of the trace elements
448 listed above for simulated seawater of various compositions: note, although the initial BIF precipitate
449 was likely a silica-rich ferrihydrite, or a ferric-silica gel (e.g., Zheng et al., 2016), there are no metal
450 binding constants available for such a mineral phase. We then calculate the adsorptive loads
451 associated with the amount of ferrihydrite estimated to have been deposited annually (7.85×10^{11}
452 moles). In Figure 1B we present the case for simulated seawater containing trace elements in
453 photoferrotroph-like proportions to mimic a Paleoproterozoic water column where – like today - trace
454 elemental ratios in seawater reflect the average composition of phytoplankton (Sunda, 2012). We find
455 that at low sorbent/sorbate ratios (low concentrations of ferrihydrite), sorption is incomplete, and
456 surface adsorbed species are fractionated relative to the original fluid (Figure 1B). As the
457 sorbent/sorbate ratio is increased, surface concentrations on ferrihydrite decrease (c.f. the trend to
458 lower elemental exit fluxes with increasing local ferrihydrite concentrations in Figure 1B), however,
459 elemental fractionation no longer occurs between ferrihydrite and the aqueous phase as sorption tends
460 to 100% of available trace elements. In our adsorption models, this occurs between 500 and 5000

461 ppm Fe as ferrihydrite (Figure 1B). Such high ferrihydrite concentrations represent systems far from
462 equilibrium with respect to solubility limits on dissolved Fe(II).

463 With oxyhydroxide settling in the water column these high sorbent/sorbate ratios are unlikely
464 to have been met. However, quantitative sorption by ferrihydrite would take on a critical role in the
465 sedimentary in the uppermost portion of the sediment pile and during later diagenesis when cell
466 biomass was degraded and biomass-associated trace elements were liberated to the sediment pore-
467 waters. In theory, oxide particle aggregation could also lead to local microenvironments with
468 quantitative sorption, although this has not been demonstrated in modern ferruginous environments.

469 One issue that workers using BIF as paleo-seawater proxies confront is whether the trace
470 element concentrations in BIF are primary. Although it is possible to avoid analyzing BIF that have
471 undergone secondary enrichments by sampling rocks with preservation of sub-mm scale primary
472 sedimentary bedding and avoiding rocks with veining, recrystallized chert, martite formation etc., it
473 is more difficult to constrain what trace elements may have left the system during early diagenesis
474 and burial. In this regard, the effectiveness of ferrihydrite at high concentrations to remove trace
475 elements from pore water, and the fact that they retain the trace element enrichment pattern
476 resembling that of the source (in this case, seawater with trace elements in photoferrotroph–like
477 proportions to simulate decaying biomass; Figure 1B; Table 1), suggests that remobilization out of
478 the sediments during burial is unlikely to have been of primary importance in controlling trace
479 element signatures.

480 ***Recycling of photoferrotrophic biomass and nutrient supply***

481 The idea that a standing population of phytoplankton may have undergone one hundred or more
482 population renewals through the course of the year has profound consequences for Fe recycling and
483 the Fe:C ratio of the BIF sediments. Both photoferrotrophy [reaction 1] and DIR [reaction 2] maintain

484 a 4:1 Fe:C molar ratio, so for ferric iron to be preserved in BIF as hematite and magnetite, the former
485 must be deposited in a molar ratio with C that is in excess of 4:1 (Konhauser et al., 2005).

486 $$[1]\ 4Fe^{2+} + CO_2 + 11H_2O \rightarrow CH_2O + 4Fe(OH)_3 + 8H^+$$

487 $$[2]\ CH_3COO^- + 8Fe(OH)_3 \rightarrow 8Fe^{2+} + 2HCO_3^- + 15OH^- + 5H_2O$$

488 This is achievable in two ways. First, some modern photoferrotrophic cells have been shown
489 in experiments to remain in suspension after Fe(II) oxidation, with ferric iron particles preferentially
490 settling out (Posth et al., 2010; Gauger et al., 2016). This implies that during times of BIF deposition,
491 such particles would have settled to the seafloor without the stoichiometric proportion of the cell
492 biomass that produced them. Crucially, separated from its correspondent oxidant, and in the absence
493 of sulfate in the Archean ocean (Crowe et al., 2014), this biomass would ultimately have been tied to
494 another form of microbial respiration, such as methanogenesis (Konhauser et al., 2005), or would
495 have been buried in carbon-rich oxidant-poor sediments, such as black shales (Thompson et al., in
496 review).

497 Second, much of the biomass (including cyanobacteria, other phototrophs and non-
498 phototrophs) was degraded prior to burial and DIR. Today, global organic carbon burial efficiencies
499 are well below ~1% of net marine primary productivity (Raven and Falkowski, 1999), with most
500 organic carbon respired using dissolved oxygen or sulfate as the terminal electron acceptors
501 (Middleburg et al., 1993). With much lower dissolved oxygen and sulfate levels than the modern, it
502 is thus likely that DIR was the predominant respiratory process during BIF deposition. Based on the
503 potential amount of biomass generated photoferrotrophically with the reducing equivalents required
504 for magnetite formation, Konhauser et al. (2005) hypothesized that 3% of the phytoplankton biomass
505 was buried and then oxidized in the sediment pile via DIR. More recent estimates using the C isotope

506 and magnetite mass balance in BIF have put initial C_{org} burial efficiencies at nearly 5% (Li et al.,
507 2013).

508 An important consideration in our model is that if only 5% of the organic carbon produced by
509 plankton was buried and then oxidized via DIR, the other 95% was degraded by other processes (e.g.,
510 fermentation, methanogenesis) while settling through the shallow water column (~100 m for the
511 continental shelf) or most likely, while deposited at the seafloor. The importance of the latter two
512 metabolisms cannot be overstated because both result in the removal of biomass in the form of
513 fermentation products (e.g., H_2, lactate, acetate, CO_2) or methane gas, but with the trace elements
514 originally sorbed to the biomass now liberated into the pore waters. Indeed, in modern anoxic tidal
515 flats ^{13}C-labelled glucose was shown to be almost completely fermented within just two days to
516 acetate, ethanol, formate and H_2 (Graue et al., 2012). Moreover, in Kabuno Bay, DR Congo,
517 fermentation, sulfate reduction, and methanogenesis occur alongside DIR, and the net result is that
518 ferric oxyhydroxides escape reduction and make it to the sediment pile (Llirós et al., 2015).

519 In short, we argue that decaying biomass was likely an important source of trace elements to
520 the Dales Gorge Member, and that standing stocks of phytoplankton, especially photoferrotrophic
521 biomass, would have been capable of supplying this flux. Remineralization of their biomass
522 subsequently liberated significant quantities of trace elements back into the water column and into
523 pore-waters to feed further growth. Interestingly, many trace elements in modern marine
524 environments exhibit nutrient-like behaviour (e.g., Cd, Cu, Ni, Zn), meaning that they are generally
525 drawn down to nanomolar concentrations in the photic zone because of biological utilization. With
526 depth in the water column they are then liberated from sinking biomass via grazing and organic matter
527 remineralization (Suess, 1980; Henrichs and Reeburgh, 1987), thus leading to their regeneration and
528 enrichment in deeper waters at elemental ratios reflecting the average composition of phytoplankton
529 (e.g., Bruland and Lohan, 2003; Sunda, 2012; Biller and Bruland, 2013). Accordingly, there is a

strong correlation between intracellular and dissolved seawater elemental stoichiometries in modern marine environments (Moore et al., 2013). As these deeper waters are again brought onto the shelf, the trace elements fuel further picoplanktonic growth. However, where BIF depositional settings differ is that they formed in relatively shallow waters where recycling would have taken place at the seafloor and where the accumulated mass of precursor phases to BIF (ferric oxyhydroxides) then acquired the biologically-controlled trace element stoichiometries in bottom water or porewaters. This acquisition could have occurred through particle aggregation and progressive element capture or during mineral aging with trace element exchange during particle settling. Either ways we propose that through these processes BIF themselves became a permanent recorder of ancient phytoplanktonic activity.

CONCLUSIONS

The strong biological requirement for trace elements by marine phytoplankton promotes the export of these elements from the photic zone. Using new constraints on trace element assimilation and adsorption by photoferrotrophs, we demonstrate that photoferrotroph populations in the past would have cycled annual amounts of trace elements that are comparable to the total BIF exit flux. Remineralization through a combination of fermentation, DIR, and methanogenesis then liberated significant quantities of trace elements back into the pore-waters where near quantitative sorption by the vast amounts of deposited ferrihydrite would have locked those trace elements into the BIF record. While adsorption to iron minerals remains an important mechanism for the ultimate capture of trace elements in BIF precursor sediments, the same photoferrotroph populations implicated in BIF deposition should have cycled the entirety of these trace elements through their biomass prior to BIF

551 deposition, suggesting a new role for BIF archives as a potential recorder of ancient phytoplanktonic
552 activity.

553 **ACKNOWLEDGMENTS**

554 This work was supported by a Natural Sciences and Engineering Research Council of Canada award
555 to KOK, DSA, MKG and SAC, as well as the European Institute for Marine Studies (LabexMER,
556 ANR-10-LABX-19) to SVL. LJR gratefully acknowledges the support of a Vanier Canada Graduate
557 Scholarship. AK was supported by the European Research Council under the European Union
558 Seventh Framework Program (FP/2007-2013)/ERC grant agreement 307320-MICROFOX. EDS was
559 supported by an NSF International Research Fellowship (1064391). Core samples from the Dales
560 Gorge Member were provided by Geological Survey of Western Australia.

561

562 **REFERENCES CITED**

563 Ahn, J.H., and Buseck, P.R., 1990, Hematite nanospheres of possible colloidal origin from a
564 Precambrian banded iron formations: Science, v. 250, p. 111-113.
565 Alibert, C., and McCulloch, M., 1993, Rare earth element and neodymium isotopic compositions of
566 the banded iron-formations and associated shales from Hamersley, western Australia:
567 Geochimica et Cosmochimica Acta, v. 57, p. 187–204.
568 Bekker, A., Planavsky, N.J., Krapež, B., Rasmussen, B., Hofmann, A., Slack, J.F., Rouxel, O.J., and
569 Konhauser, K.O., 2014, Iron formation: Their origins and implications for ancient seawater
570 chemistry: In: H.D. Holland and K.K. Turkian (Editors), Treatise in Geochemistry, 2nd
571 Edition, Elsevier, Amsterdam, pp. 561-628.
572 Bekker, A., Slack, J.F., Planavsky, N., Krapež, B., Hofmann, A., Konhauser, K.O., and Rouxel, O.J.,
573 2010. Iron formation: A sedimentary product of the complex interplay among mantle, tectonic,
574 and biospheric processes: Economic Geology, v. 105, p. 467-508.
575 Biebl, H., and Pfennig, N., 1978, Growth yields of green sulfur bacteria in mixed cultures with sulfur
576 and sulfate reducing bacteria: Journal of Microbiology, v. 117, p. 9-16.
577 Biller, D.V., and Bruland, K.W., 2013, Sources and distributions of Mn, Fe, Co, Ni, Cu, Zn, and Cd
578 relative to macronutrients along the central California coast during the spring and summer
579 upwelling season: Marine Chemistry, v. 155, p. 50–70, doi: 10.1016/j.marchem.2013.06.003.
580 Bjerrum, C.J., and Canfield, D.E., 2002, Ocean productivity before about 1.9 Gyr ago limited by
581 phosphorus adsorption onto iron oxides: Nature, v. 417, p. 159–162, doi: 10.1038/417159a.
582 Blättler, C.L., Kump, L.R., Fischer, W.W., Paris, G., Kasbohm, J.J., and Higgins, J.A., 2016,
583 Constraints on ocean carbonate chemistry and pCO2 in the Archaean and Palaeoproterozoic:
584 Nature Geoscience, v. 10, p. 41–45, doi:10.1038/ngeo2844.
585 Borrok, D.M., Fein, J.B., and Kulpa, C.F., 2004a, Cd and proton adsorption onto bacterial consortia

586 grown from industrial wastes and contaminated geologic settings: Environmental Science &
587 Technology, v. 38, p. 5656–5664, doi: 10.1021/es049679n.
588 Borrok, D., Fein, J.B., and Kulpa, C.F., 2004b, Proton and Cd adsorption onto natural bacterial
589 consortia: Testing universal adsorption behavior: Geochimica et Cosmochimica Acta, v. 68,
590 p. 3231–3238, doi: 10.1016/j.gca.2004.02.003.
591 Bruland, K.W., Donat, J.R., and Hutchins, D.A., 1991, Interactive influences of bioactive trace metals
592 on biological production in oceanic waters: Limnology and Oceanography, v. 36, p. 1555–
593 1577, doi: 10.4319/lo.1991.36.8.1555.
594 Bruland, K.W., 1992, Complexation of cadmium by natural organic ligands in the central North
595 Pacific: Limnology and Oceanography, v. 37, p. 1008-1017, doi: 10.4319/lo.1992.37.5.1008.
596 Bruland, K.W., and Lohan, M.C., 2003, Controls of trace metals in seawater, *in* Holland, H.D. and
597 Turekian, K. eds., Treatise on Geochemistry, Elsevier, v. 6, p. 23–47, doi: 10.1016/b0-08-
598 043751-6/06105-3.
599 Byrne, R.H., Kump, L.R., and Cantrell, K.J., 1988, The influence of temperature and pH on trace
600 metal speciation in seawater: Marine Chemistry, v. 25, p. 163–181, doi: 10.1016/0304-
601 4203(88)90062-x.
602 Capone, D.G., Zehr, J.P., Paerl, H.W., Bergman, B., and Carpenter, E.J., 1997, *Trichodesmium*, a
603 globally significant marine cyanobacterium: Science, v. 276**,** p. 1221–1229.
604 Chan, C.S., Emerson, D., and Luther, G.W., 2016, The role of microaerophilic Fe-oxidizing micro-
605 organisms in producing banded iron formations: Geobiology, v. 14, p. 509-528, doi:
606 10.1111/gbi.12192.
607 Cloud, P., 1973, Paleoecological significance of the banded iron-formation: Economic Geology, v.
608 68, p. 1135–1143.
609 Crowe, S.A., Jones, C., Katsev, S., Magen, C., O'Neill, A., Sturm, A., Canfield, D., Haffner, G.,

610 Mucci, A., and Sundby, B., 2008, Photoferrotrophs thrive in an Archean Ocean analogue:
611 Proceedings of the National Academy of Sciences USA, v. 105, p. 15938–15943.
612 Crowe, S.A., Katsev, S., Leslie, K., Sturm, A., Magen, C., Nomosatryo, S., Pack, M.A., Kessler, J.D.,
613 Reeburgh, W.S., Roberts, J.A., González, L., Haffner, G.D., Mucci, A., Sundby, B., et al.,
614 2011, The methane cycle in ferruginous Lake Matano: Geobiology, v. 9, p. 61–78, doi:
615 10.1111/j.1472-4669.2010.00257.x.
616 Crowe, S.A., Paris, G., Katsev, S., Jones, C., Kim, S.-T., Zerkle, A.L., Nomosatryo, S., Fowle, D.A.,
617 Adkins, J.F., Sessions, A.L., Farquhar, J., and Canfield, D.E., 2014, Sulfate was a trace
618 constituent of Archean seawater: Science, v. 346, p. 735–739, doi: 10.1126/science.1258966.
619 Dittrich, M., and Sibler, S., 2005, Cell surface groups of two picocyanobacteria strains studied by
620 zeta potential investigations, potentiometric titration, and infrared spectroscopy: Journal of
621 Colloid and Interface Science, v. 286, p. 487–495, doi: 10.1016/j.jcis.2005.01.029.
622 Dzombak, D.A., and Morel, F.M.M., 1990, Surface Complexation Modeling: Wiley-Interscience, p.
623 1–393.
624 Ehrenreich, A., and Widdel, F., 1994, Anaerobic oxidation of ferrous iron by purple bacteria, a new
625 type of phototrophic metabolism: Applied and Environmental Microbiology, v. 60, p. 4517–
626 4526.
627 Eickhoff, M., Obst, M., Schröder, C., Hitchcock, A.P., Tyliszczak, T., Martinez, R.E., Robbins, L.J.,
628 Konhauser, K.O., and Kappler, A., 2014, Nickel partitioning in biogenic and abiogenic
629 ferrihydrite: The influence of silica and implications for ancient environments: Geochimica et
630 Cosmochimica Acta, v. 140, p. 65–79, doi: 10.1016/j.gca.2014.05.021.
631 Ewers, W.E., and Morris, R.C., 1981, Studies of the Dales Gorge Member of the Brockman Iron
632 Formation, Western Australia: Economic Geology, v. 76, p. 1929-1953.
633 Fein, J., Martin, A., and Wightman, P., 2001, Metal adsorption onto bacterial surfaces: Development

of a predictive approach: Geochimica et Cosmochimica Acta, v. 65, p. 4267–4273.

Frei, R., Crowe, S.A., Bau, M., Polat, A., Fowle, D.A., and Døssing, L.N., 2016, Oxidative elemental cycling under the low O2 Eoarchean atmosphere: Scientific Reports, v. 6, p. 1–9, doi: 10.1038/srep21058.

Fru, E.C., Rodríguez, N.P., Partin, C.A., Lalonde, S., Andersson, P., Weiss, D.J., Abderazzak, E.A., Rodushkin, I., and Konhauser, K.O., 2016, Cu isotopes in marine black shales record the Great Oxidation Event: Proceedings of the National Academy of Sciences USA, v. 113, p. 4941-4946.

Garrels, R.M., and Perry, E.A.J., 1974, Cycling of carbon, sulfur, and oxygen through geologic time, *in* Goldberg, E.A., ed., The Sea: New York, Wiley, p. 303-336.

Gauger, T., Byrne, J.M., Konhauser, K.O., Obst, M., Crowe, S.A., and Kappler, A., 2016, Influence of organics and silica on Fe(II) oxidation rates and cell–mineral aggregate formation by the green-sulfur Fe(II)-oxidizing bacterium *Chlorobium ferrooxidans* KoFox – Implications for Fe(II) oxidation in ancient oceans: Earth and Planetary Science Letters, v. 443, p. 81–89, doi: 10.1016/j.epsl.2016.03.022.

Graue, J., Engelen, B., and Cypionka, H., 2012, Degradation of cyanobacterial biomass in anoxic tidal-flat sediments: a microcosm study of metabolic processes and community changes: Multidisciplinary Journal of Microbial Ecology, v. 6, p. 660-669.

Grotzinger, J.P., and Kasting, J.F., 1993, New constraints on Precambrian ocean composition: The Journal of Geology, v. 101, p. 235–243, doi:10.1086/648218.

Gustafsson, J.P., 2013, Visual Minteq: http://www.lwr.kth.se/English/OurSoftware/vminteq/ (accessed April 2017).

Hadjoudja, S., Deluchat, V., and Baudu, M., 2010, Cell surface characterisation of *Microcystis aeruginosa* and *Chlorella vulgaris*: Journal of Colloid and Interface Science, v. 342, p. 293–

299, doi: 10.1016/j.jcis.2009.10.078.

Hallbeck, L., and Pedersen, K., 1991, Autotrophic and mixotrophic growth of *Gallionella ferruginea*: Microbiology, v. 137, p. 2657–2661, doi: 10.1099/00221287-137-11-2657.

Han, T.M., 1988, Origin of magnetite in Precambrian iron-formations of low metamorphic grade: In: Zachrisson E., ed, Proceedings of the Seventh Quadrennial IAGOD Symposium: Stuttgart, E. Schweizerbart'che Verlagsbachhandlung, p.641-656.

Hao, L., Li, J., Kappler, A., and Obst, M., 2013, Mapping of heavy metal ion sorption to cell-extracellular polymeric substance-mineral aggregates by using metal-selective fluorescent probes and confocal laser scanning microscopy: Applied and Environmental Microbiology, v. 79, p. 6524-6534.

Hegler, F., Posth, N.R., Jiang, J., and Kappler, A., 2008, Physiology of phototrophic iron(II)-oxidizing bacteria: implications for modern and ancient environments: FEMS Microbiology Ecology, v. 66, p. 250-260.

Heimann, A., Johnson, C.M., Beard, B.L., Valley, J.W., Roden, E.E., Spicuzza, M.J., and Beukes, N.J., 2010, Fe, C, and O isotope compositions of banded iron formation carbonates demonstrate a major role for dissimilatory iron reduction in ~ 2.5 Ga marine environments: Earth and Planetary Science Lett, v. 294, p. 8-18.

Henrichs, S.M., and Reeburgh, W.S., 1987, Anaerobic mineralization of marine sediment organic matter: Rates and the role of anaerobic processes in the oceanic carbon economy: Geomicrobiology Journal, v. 5, p. 191–237, doi: 10.1080/01490458709385971.

Ho, T.Y., Quigg, A., Finkel, Z.V., Milligan, A.J., Wyman, K., Falkowski, P.G., and Morel, F.M.M., 2003, The elemental composition of some marine phytoplankton: Journal of Phycology, v. 39, p. 1145–1159, doi: 10.1111/j.0022-3646.2003.03-090.x.

Jacquet, S., Lennon, J.-F., Marie, D., and Vaulot, D., 1998, Picoplankton population dynamics in

682 coastal waters of the northwestern Mediterranean Sea: Limnology and Oceanography, v. 43,
683 p. 1916–1931, doi: 10.4319/lo.1998.43.8.1916.
684 James, H.L., 1954, Sedimentary facies of iron-formation: Economic Geology, v. 49, p. 235−293.
685 Johnson, C.M., Beard, B.L., Klein, C., Beukes, N.J., and Roden, E.E., 2008b. Iron isotopes constrain
686 biologic and abiologic processes in banded iron formation genesis. Geochimica et
687 Cosmochimica Acta, 72:151-169.
688 Jones, C., Nomosatryo, S., Crowe, S.A., Bjerrum, C.J., and Canfield, D.E., 2015, Iron oxides, divalent
689 cations, silica, and the early earth phosphorus crisis: Geology, v. 43, p. 135–138, doi:
690 10.1130/G36044.1.
691 Kappler, A., Pasquero, C., Konhauser, K.O., and Newman, D.K., 2005, Deposition of banded iron
692 formations by anoxygenic phototrophic Fe(II)-oxidizing bacteria: Geology, v. 33, p. 865–868,
693 doi: 10.1130/G21658.1.
694 Köhler, I., Konhauser, K.O., and Kappler, A., 2010, Role of microorganisms in banded iron
695 formations, *in* Geomicrobiology: Molecular and Environmental Perspective, Springer Science
696 + Business Media, p. 309–324, doi: 10.1007/978-90-481-9204-5_14.
697 Köhler, I., Konhauser, K.O., Papineau, D., Bekker, A., and Kappler, A., 2013, Biological carbon
698 precursor to diagenetic siderite with spherical structures in iron formations. Nature
699 Communications: v. 4, p. 1741-1747.
700 Konhauser, K.O., Hamade, T., Raiswell, R., Morris, R., Ferris, F., Southam, G., and Canfield, D.,
701 2002, Could bacteria have formed the Precambrian banded iron formations?: Geology, v. 30,
702 p. 1079–1082.
703 Konhauser, K.O., Newman, D., and Kappler, A., 2005, The potential significance of microbial Fe
704 (III) reduction during deposition of Precambrian banded iron formations: Geobiology, v. 3, p.
705 167–177.

706 Konhauser, K.O., Lalonde, S.V., Amskold, L.A., and Holland, H., 2007a, Was there really an Archean
707 phosphate crisis?: v. 315, p. 1234.
708 Konhauser, K.O., Amskold, L.A., Lalonde, S.V., Posth, N., Kappler, A., and Anbar, A.D., 2007b,
709 Decoupling photochemical Fe (II) oxidation from shallow-water BIF deposition: Earth and
710 Planetary Science Letters, v. 258, p. 87–100, doi:10.1016/j.epsl.2007.03.026.
711 Konhauser, K.O., Pecoits, E., Lalonde, S.V., Papineau, D., Nisbet, E.G., Barley, M.E., Arndt, N.T.,
712 Zahnle, K., and Kamber, B.S., 2009, Oceanic nickel depletion and a methanogen famine
713 before the Great Oxidation Event: Nature Geoscience, v. 458, p. 750–753, doi:
714 10.1038/nature07858.
715 Konhauser, K.O., Lalonde, S.V., Planavsky, N.J., Pecoits, E., Lyons, T.W., Mojzsis, S.J., Rouxel,
716 O.J., Barley, M.E., Rosière, C.A., Fralick, P.W., Kump, L.R., and Bekker, A., 2011, Aerobic
717 bacterial pyrite oxidation and acid rock drainage during the Great Oxidation Event: Nature
718 Geoscience, v. 478, p. 369–373, doi: 10.1038/nature10511.
719 Konhauser, K.O., Robbins, L.J., Pecoits, E., Peacock, C., Kappler, A., and Lalonde, S.V., 2015, The
720 Archean nickel famine revisited: Astrobiology, v. 15, p. 804-815.
721 Krapež, B., Barley, M.E., and Pickard, A.L., 2003, Hydrothermal and resedimented origins of the
722 precursor sediments to banded iron formations: sedimentological evidence from the Early
723 Palaeoproterozoic Brockman Supersequence of Western Australia: Sedimentology, v. 50, p.
724 979-1011.
725 Kuntz, L.B., Laakso, T.A., Schrag, D.P., and Crowe, S.A., 2015, Modeling the carbon cycle in Lake
726 Matano: Geobiology, v. 13, p. 454–461, doi: 10.1111/gbi.12141.
727 Li, W., Huberty, J., Beard, B., Valley, J., Johnson, C., 2013. Contrasting behavior of oxygen and iron
728 isotopes in banded iron formations as determined by *in situ* isotopic analysis. Earth and
729 Planetary Science Letters 384, 132-143.

730 Li, Y.L., Konhauser, K.O., Cole, D.R., and Phelps, T.J., 2011, Mineral ecophysiological data provide
731 growing evidence for microbial activity in banded-iron formations: Geology, v. 39, p. 707–
732 710, doi: 10.1130/G32003.1.
733 Liu, Y., Alessi, D.S., Owttrim, G.W., and Petrash, D.A., 2015, Cell surface reactivity of
734 *Synechococcus* sp. PCC 7002: Implications for metal sorption from seawater: Geochimica et
735 Cosmochimica Acta, v. 169, p. 30–44, doi: 10.1016/j.gca.2015.07.033.
736 Llirós, M., Armisen, T.G., Darchambeau, F., Morana, C., Margarit, X.T., Inceoğlu, Ö., Borrego,
737 C.M., Bouillon, S., Servais, P., Borges, A.V., Descy, J.P., Canfield, D.E., and Crowe, S.A.,
738 2015, Pelagic photoferrotrophy and iron cycling in a modern ferruginous basin: Nature
739 Publishing Group, p. 1–8, doi: 10.1038/srep13803.
740 Martell, A. E., Smith, R. M., 1977, *Critical Stability Constants*, Vol. 3, Other Organic Ligands,
741 Plenum, New York, NY.
742 Martinez, R.E., Konhauser, K.O., Paunova, N., Wu, W., Alessi, D.S., and Kappler, A., 2016, Surface
743 reactivity of the anaerobic phototrophic Fe(II)-oxidizing bacterium *Rhodovulum iodosum*:
744 implications for trace metal budgets in ancient oceans and banded iron formations: Chemical
745 Geology, v. 442, p. 113-120, doi: 10.1016/j.chemgeo.2016.009.004.
746 Middelburg, J.J., Vlug, T., Jaco, F., and van der Nat, W.A., 1993, Organic matter mineralization in
747 marine systems: Global and Planetary Change, v. 8, p. 47–58, doi: 10.1016/0921-
748 8181(93)90062-s.
749 Mikutta, R., Baumgärtner, A., Schippers, A., Haumaier, L., and Guggenberger, G., 2012,
750 Extracellular polymeric substances from *Bacillus subtilis* associated with minerals modify the
751 extent and rate of heavy metal sorption: Environmental Science & Technology, v. 46, p. 3866–
752 3873, doi: 10.1021/es204471x.
753 Miyazono, A., Odate, T., and Maita, Y., 1992, Seasonal fluctuations of cell density of cyanobacteria

754 and other picophytoplankton in Iwanai Bay, Hokkaido, Japan: Journal of Oceanography, v.
755 48, p. 257–266, doi: 10.1007/bf02233986.

756 Moon, E.M., and Peacock, C.L., 2013, Modelling Cu(II) adsorption to ferrihydrite and ferrihydrite–
757 bacteria composites: Deviation from additive adsorption in the composite sorption system:
758 Geochimica et Cosmochimica Acta, v. 104, p. 148–164, doi: 10.1016/j.gca.2012.11.030.

759 Moore, C.M., Mills, M.M., Arrigo, K.R., Berman-Frank, I., Bopp, L., Boyd, P.W., Galbraith, E.D.,
760 Geider, R.J., Guieu, C., Jaccard, S.L., Jickells, T.D., La Roche, J., Lenton, T.M., Mahowald,
761 N.M., et al., 2013, Processes and patterns of oceanic nutrient limitation: Nature Geoscience,
762 v. 6, no. 9, p. 701–710, doi: 10.1038/ngeo1765.

763 Nuester, J., Vogt, S., Newville, M. Kustka, A.B., and Twining, B. S., 2012, The unique
764 biogeochemical signature of the marine diazotroph Trichodesmium. *Environmental*
765 *Bioinorganic Chemistry of Aquatic Microbial Organisms*, v. 164 doi:
766 10.3389/fmicb.2012.00150.

767 Olson, S.L., Kump, L.R., and Kasting, J.F., 2013, Quantifying the areal extent and dissolved oxygen
768 concentrations of Archean oxygen oases: Chemical Geology, v. 362, p. 35–43, doi:
769 10.1016/j.chemgeo.2013.08.012.

770 Pai, S.C., and Chen, H.Y., 1994, Vertical distribution of cadmium in marginal seas of the western
771 Pacific Ocean: Marine Chemistry, v. 47, p. 81–91, doi: 10.1016/0304-4203(94)90015-9.

772 Pecoits, E., Gingras, M.K., Barley, M.E., Kappler, A., Posth, N., and Konhauser, K.O., 2009,
773 Petrography and geochemistry of the Dales Gorge banded iron formation: Paragenetic
774 sequence, source and implications for palaeo-ocean chemistry: Precambrian Research, v. 172,
775 p. 163–187.

776 Pecoits, E., Smith, M.L., Catling, D.C., Philippot, P., Kappler, A., and Konhauser, K.O., 2015,

777 Atmospheric hydrogen peroxide and Eoarchean iron formations: Geobiology, v. 13, p. 1–14,
778 doi:10.1111/gbi.12116.
779 Percak-Dennett, L., Roden, E.E., Beard, B.L., and Johnson, C.M., 2011, Iron isotope fractionation
780 during dissimilatory iron reduction under simulated Archean conditions. Geobiology 9, 205-
781 220.
782 Planavsky, N.J., 2014, The elements of marine life: Nature Geoscience, v. 7, p. 855–856.
783 Planavsky, N., Rouxel, O.J., Bekker, A., Hofmann, A., Little, C.T.S., Lyons, T.W., 2012. Iron isotope
784 composition of some Archean and Proterozoic iron formations. Geochimica et Cosmochimica
785 Acta 80, 158-169.
786 Planavsky, N.J., Asael, D., Hofmann, A., Reinhard, C.T., Lalonde, S.V., Knudsen, A., Wang, X.,
787 Ossa Ossa, F., Pecoits, E., Smith, A.J.B., Beukes, N.J., Bekker, A., Johnson, T.M., Konhauser,
788 K.O., et al., 2014, Evidence for oxygenic photosynthesis half a billion years before the Great
789 Oxidation Event: Nature Geoscience, v. 7, p. 283–286, doi: 10.1038/ngeo2122.
790 Posth, N.R., Huelin, S., Konhauser, K.O., and Kappler, A., 2010, Size, density and composition of
791 cell–mineral aggregates formed during anoxygenic phototrophic Fe(II) oxidation: Impact on
792 modern and ancient environments: Geochimica et Cosmochimica Acta, v. 74, p. 3476–3493,
793 doi: 10.1016/j.gca.2010.02.036.
794 Posth, N.R., Konhauser, K.O., and Kappler, A., 2013, Microbiological processes in banded iron
795 formation deposition: Sedimentology, v. 60, p. 1733–1754, doi: 10.1111/sed.12051.
796 Price, N.M., and Morel, F.M.M., 1990, Cadmium and cobalt substitution for zinc in a marine diatom:
797 Nature Geoscience, v. 344, p. 658–660.
798 Rasmussen, B., Krapež, B., Muhling, J.R., Suvorova, A., 2015, Precipitation of iron silicate
799 nanoparticles in early Precambrian oceans marks Earth's first iron age: Geology, v. 43, p. 303–
800 306, doi:10.1130/G36309.1.

801 Rasmussen, B., Muhling, J.R., Suvorova, A., Krapež, B., 2016, Dust to dust: Evidence for the
802 formation of "primary" hematite dust in banded iron formations via oxidation of iron silicate
803 nanoparticles: Precambrian Research, v. 284, p. 49–63, doi:10.1016/j.precamres.2016.07.003.
804 Rasmussen, B., Muhling, J.R., Suvorova, A., Krapež, B., 2017, Greenalite precipitation linked to the
805 deposition of banded iron formations downslope from a late Archean carbonate platform:
806 Precambrian Research, v. 290, p. 49–62, doi:10.1016/j.precamres.2016.12.005.
807 Raven, J.A., and Falkowski, P.G., 1999, Oceanic sinks for atmospheric CO_2: Plant, Cell &
808 Environment, v. 22, p. 741–755, doi: 10.1046/j.1365-3040.1999.00419.x.
809 Reddy, T.R., Zheng, X.-Y., Roden, E.E., Beard, B.L., and Johnson, C.M., 2016. Silicon isotope
810 fractionation during microbial reduction of Fe(III)-Si gels under Archean seawater
811 conditions and implications for iron formation genesis: Geochimica et Cosmochimica Acta,
812 v. 190, p. 85-99.
813 Reinhard, C.T., Planavsky, N.J., Gill, B.C., Ozaki, K., Robbins, L.J., Lyons, T.W., Fischer, W.W.,
814 Wang, C., Cole, D.B., and Konhauser, K.O., 2017, Evolution of the global phosphorous
815 cycle: Nature, v. 541, p. 386–389.
816 Robbins, L.J., Lalonde, S.V., Saito, M.A., Planavsky, N.J., Mloszewska, A.M., Pecoits, E., Scott, C.,
817 Dupont, C.L., Kappler, A., and Konhauser, K.O., 2013, Authigenic iron oxide proxies for
818 marine zinc over geological time and implications for eukaryotic metallome
819 evolution: Geobiology, v. 11, p. 295-306.
820 Saito, M.A., Sigman, D.M, and Morel, F.M.M., 2003, The bioinorganic chemistry of the ancient
821 ocean: the co-evolution of cyanobacterial metal requirements and biogeochemical cycles at
822 the Archean-Proterozoic boundary?: Inorganica Chimica Acta, v. 356, p. 308-318.
823 Sañudo-Wilhelmy, S.A., Tovar-Sanchez, A., and Fu, F.X., 2004, The impact of surface-adsorbed
824 phosphorus on phytoplankton Redfield stoichiometry: Nature, v. 432, p. 897–901, doi:

10.1038/nature03125.

Satkoski, A.M., Beukes, N.J., Li, W., Beard, B.L., and Johnson, C.M., 2015, A redox-stratified ocean 3.2 billion years ago: Earth and Planetary Science Letters, v. 430, p. 43–53, doi: 10.1016/j.epsl.2015.08.007.

Scott, C.T., Planavsky, N.J., Dupont, C.L., Kendall, B., Gill, B.C., Robbins, L.J., Husband, K.F., Arnold, G.L., Wing, B.A., Poulton, S.W., Bekker, A., Anbar, A.D., Konhauser, K.O., and Lyons, T.W., 2013, Bioavailability of zinc in marine systems through time: Nature Geosciences, v. 6, p. 125-128.

Straub, K., Rainey, F., and Widdel, F., 1999, *Rhodovulum iodosum* sp. nov. and *Rhodovulum robiginosum* sp. nov., two new marine phototrophic ferrous-iron-oxidizing purple bacteria: International Journal of Systematic Bacteriology, v. 49, p. 729–735.

Suess, E., 1980, Particulate organic carbon flux in the oceans—surface: Nature, v. 288, p. 260–263, doi: 10.1038/288260a0.

Sun, S., Konhauser, K.O., Kappler, A., and Yiliang, L., 2015, Primary hematite in Neoarchean to Paleoproterozoic oceans: Geological Society of America Bulletin, v. 127, p. 850-861, doi:10.1130/B31122.1

Sunda, W.G., 2012, Feedback interactions between trace metal nutrients and phytoplankton in the ocean: Frontiers in Microbiology, v. 3, p. 1-22, doi: 10.3389/fmicb.2012.00204.

Swanner, E.D., Planavsky, N., Lalonde, S.V., Robbins, L.J., Bekker, A., Rouxel, O., Saito, M.A., Kappler, A., Mojzsis, S.J., and Konhauser, K.O., 2014, Cobalt and marine redox evolution: Earth and Planetary Science Letters, v. 390, p. 253-263.

Swanner, E.D., Mloszewska, A.M., Cirpka, O.A., Schoenberg, R., Konhauser, K.O., and Kappler, A., 2015, Modulation of oxygen production in Archaean oceans by episodes of Fe(II) toxicity: Nature Geoscience, v. 8, p. 126-130.

849 Tang, T., Fadaei, H., and Hu, Z., 2014, Rapid evaluation of algal and cyanobacterial activities through
850 specific oxygen production rate measurement: Ecological Engineering, v. 73, p. 439–445, doi:
851 10.1016/j.ecoleng.2014.09.095.
852 Thompson, K.J., Kenward, P.A., Bauer, K.W., Michiels, C.C., Lliros, M., Kappler, A., Gauger, T.,
853 Reinhard, C.T., Konhauser, K.O., and Crowe, S.A., Photoferrotrophs primed Earth's surface
854 for oxygenation: Nature, in review.
855 Tosca, N.J., Guggenheim, S., and Pufahl, P.K., 2015, An authigenic origin for Precambrian
856 greenalite: Implications for iron formation and the chemistry of ancient seawater: Geological
857 Society of America Bulletin, v. 128, p. 511–530, doi:10.1130/b31339.1.
858 Trendall, A.F., and Blockley, J.G., 1970, The iron formations of the Precambrian Hamersley Group
859 Western Australia with special reference to the associated crocidolite: Geological Survey of
860 Western Australia Bulletin, v. 119, p. 1–366.
861 Twining, B.S., Baines, S.B., and Fisher, N.S., 2004, Element stoichiometries of individual plankton
862 cells collected during the Southern Ocean Iron Experiment (SOFeX): Limnology and
863 Oceanography, v. 49, p. 2115–2128, doi: 10.4319/lo.2004.49.6.2115.
864 Walve, J., Gelting, J., and Ingri, J., 2014, Trace metals and nutrients in Baltic Sea cyanobacteria:
865 Internal and external fractions and potential use in nitrogen fixation: Marine Chemistry, v.
866 158, p. 27–38, doi: 10.1016/j.marchem.2013.11.002.
867 Williams, P.J., le B., 1998, The balance of plankton respiration and photosynthesis in the open oceans:
868 Nature, v. 394, p. 55–57, doi: 10.1038/27878.
869 Wu, W., Swanner, E.D., Hao, L., Zeitvogel, F., Obst, M., Pan, Y., and Kappler, A., 2014,
870 Characterization of the physiology and cell-mineral interactions of the marine anoxygenic
871 phototrophic Fe(II) oxidizer *Rhodovulum iodosum*- implications for Precambrian Fe(II)
872 oxidation: FEMS Microbiology Ecology, v. 88, p. 503–515, doi: 10.1111/1574-6941.12315.

873 Yee, N., and Fein, J., 2001, Cd adsorption onto bacterial surfaces: A universal adsorption edge?:
874 Geochimica et Cosmochimica Acta, v. 65, p. 2037–2042, doi: 10.1016/s0016-7037(01)00587-
875 7.
876 Zheng, X.-Y., Beard, B.L., Reddy, T.R., Roden, E.E., and Johnson, C.M., 2016, Abiologic silicon
877 isotope fractionation between aqueous Si and Fe(III)-Si gel in simulated Archean seawater:
878 Implications for Si isotope records in Precambrian sedimentary rocks: Geochimica et
879 Cosmochimica Acta, v. 187, p. 102-122.
880
881

Figure Captions

Figure 1: (A) Comparison of the trace element exit fluxes implicated in the deposition of the 2.48 Ga Dales Gorge BIF (grey line) with annual biomass-associated trace element fluxes calculated for the photoferrotroph *Rhodovulum iodosum* for the minimal cell population (1.9 x 10^{23} cells; solid purple line) and one undergoing turnover every three days (2.31 x 10^{25} cells; stippled purple line), as well as for the average marine cyanobacterium with either minimal cell population (4.5 x 10^{20} cells; solid green line) and for one undergoing turnover every three days (5.45 x 10^{22} cells; stippled green line). (B) Exit fluxes and elemental fractionation calculated from surface complexation modelling of adsorption to varying concentrations of ferrihydrite from simulated seawater with photoferrotroph-like trace element stoichiometry. See text for details.

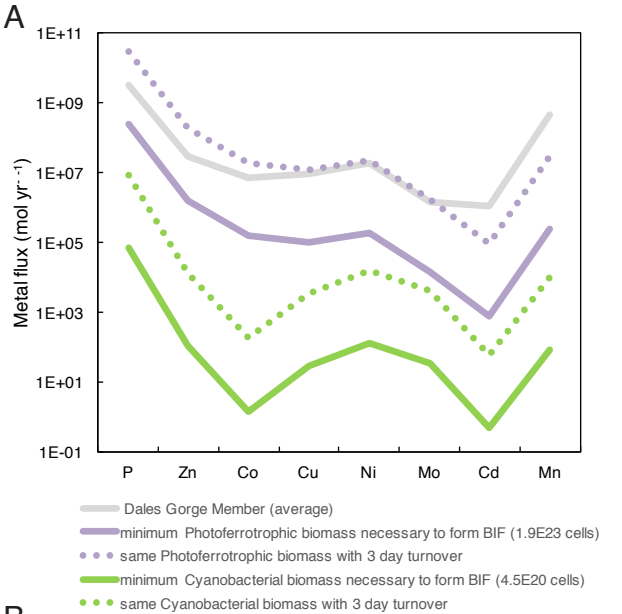
A
1E+11
1E+09
1E+07
1E+05
1E+03
1E+01
1E-01
Metal flux (mol yr⁻¹)
P
Zn
Co
Cu
Ni
Mo
Cd
Mn
Dales Gorge Member (average)
minimum Photoferrotrophic biomass necessary to form BIF (1.9E23 cells)
same Photoferrotrophic biomass with 3 day turnover
minimum Cyanobacterial biomass necessary to form BIF (4.5E20 cells)
same Cyanobacterial biomass with 3 day turnover

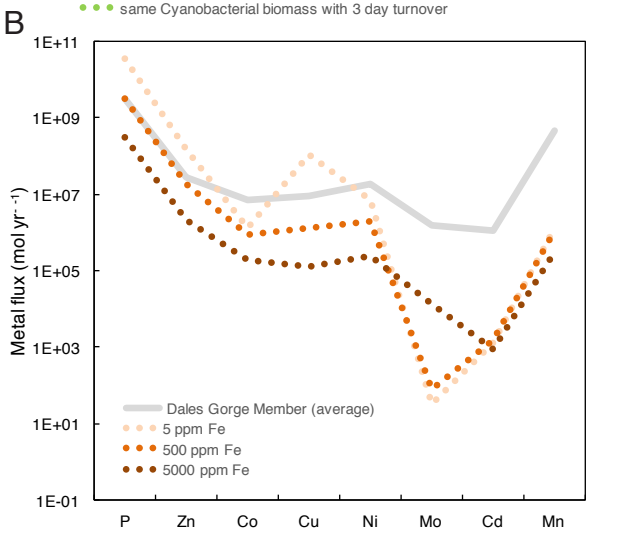
B
1E+11
1E+09
1E+07
1E+05
1E+03
1E+01
1E-01
Metal flux (mol yr⁻¹)
P
Zn
Co
Cu
Ni
Mo
Cd
Mn
Dales Gorge Member (average)
5 ppm Fe
500 ppm Fe
5000 ppm Fe